Appl Microbiol Biotechnol (2017) 101:3463–3472
DOI 10.1007/s00253-016-8087-2

ENVIRONMENTAL BIOTECHNOLOGY

Transcriptome and metabolome responses of *Shewanella oneidensis* MR-1 to methyl orange under microaerophilic and aerobic conditions

Xinhua Cao[1,2] · **Yueling Qi**[1,2] · **Chen Xu**[1,2] · **Yuyi Yang**[1] · **Jun Wang**[1,3]

Received: 11 October 2016 / Revised: 13 December 2016 / Accepted: 21 December 2016 / Published online: 9 January 2017

Abstract *Shewanella oneidensis* MR-1 degrades various azo dyes under microaerophilic and anaerobic conditions, but this process is inhibited under aerobic conditions. The mechanisms underlying azo dye biodegradation and inhibition remain unknown. Therefore, we investigated metabolic and transcriptional changes in strain MR-1, which was cultured under different conditions, to elucidate these mechanisms. At the transcriptional level, genes involved in certain metabolic processes, particularly the tricarboxylic acid (TCA) cycle, amino acid biodegradation, and the electron transfer system, were significantly altered ($M \geqq 2$, $p > 0.8$) in the presence of methyl orange (MO). Moreover, a high concentration of dissolved oxygen heavily impacted the expression levels of genes involved in fatty acid biodegradation. Metabolome analysis revealed significant alteration ($p < 0.05$) in the concentrations of nine metabolites when strain MR-1 was cultured under aerobic conditions; the majority of these metabolites were closely associated with amino acid metabolism and DNA replication. Accordingly, we propose a possible pathway for MO biodegradation and discuss the most likely causes of biodegradation inhibition due to dissolved oxygen.

Keywords Metabolome · Transcriptome · Azo dye · Dissolved oxygen · Biodegradation mechanism

Introduction

Azo dyes, whose utilization and discharge into the environment by textile industry increase annually, are currently worldwide pollutants (Jin et al. 2014; Singh and Arora 2011). Most azo dyes are toxic, mutagenic, and carcinogenic, showing potential risks to human health (Hafshejani et al. 2014; Stolz 2001). Different technologies have been developed to remediate azo dye contamination, including adsorption, membrane filtration, photocatalysis, and microbiological or enzymatic decomposition (Forgacs et al. 2004; Willetts and Ashbolt 2000). Among these, microbiological technologies are the most promising due to their low cost, high efficacy, and environmentally friendly nature (Khan et al. 2014b; Silva et al. 2014). Many microorganisms are capable of degrading azo dyes through the azo reduction process mediated by azoreductase, which is expressed in vivo by bacteria and is considered as a key enzyme (Hu 1994; Saroj et al. 2014; Silva et al. 2014; Yang et al. 2013). In most cases, complete azoreduction by bacteria is achieved under anaerobic or microaerophilic conditions, as previously observed in *Stenotrophomonas* sp. strain BHUSSp X2 (Kumari et al. 2016) and *Sphingomonas* sp. strain BN6 (Kudlich et al. 1997). However, the products generated by azoreduction under microaerophilic conditions are less toxic than those produced under aerobic conditions (Hafshejani et al. 2014; Khan et al. 2014a). Bacteria within the *Shewanella* genus, particularly *Shewanella oneidensis* MR-1, possess the ability to

Electronic supplementary material The online version of this article (doi:10.1007/s00253-016-8087-2) contains supplementary material, which is available to authorized users.

✉ Yuyi Yang
yangyy@wbgcas.cn

✉ Jun Wang
wangjun@wbgcas.cn

[1] Key Laboratory of Aquatic Botany and Watershed Ecology, Wuhan Botanical Garden, Chinese Academy of Sciences, Wuhan 430074, China

[2] University of Chinese Academy of Sciences, Beijing 100049, China

[3] Sino-Africa Joint Research Center, Chinese Academy of Sciences, Wuhan 430074, China

degrade a diverse range of azo dyes under microaerophilic conditions, such as amaranth (Le Laz et al. 2014), methyl red (Yang et al. 2013), methyl orange (MO), and naphthol green B (Cao et al. 2013). However, azo dye degradation by MR-1 is largely inhibited by dissolved oxygen (DO) (Hong et al. 2007). The mechanisms underlying the biodegradation of azo dyes by *S. oneidensis* MR-1 have not been extensively explored nor have the mechanisms underlying the inhibition by DO, particularly at metabolome and transcriptome levels. Knowledge of gene expression alterations involved in azoreduction, as well as resulting metabolite changes, will help us gain a better understanding of the mechanisms involved in azoreduction under different conditions (Tyagi et al. 2014; Wang et al. 2014; Zhang et al. 2011).

Recently, metabolomics has been widely adopted to generate profiles of endogenous small molecular compounds in living organisms exposed to exogenous stimuli (Rochfort 2005; Wishart 2005). Nuclear magnetic resonance (NMR) is preferred for metabolomic profiling compared with chromatography-mass spectrometry methods due to its simpler sample preparation procedures that result in less disturbance of intracellular metabolites (Lindon et al. 2001). NMR has been utilized by many researchers to investigate the responses of organisms to various environmental stresses, such as heavy metals (Tyagi et al. 2014), organic pollutants (Hong et al. 2014), and extreme temperatures (Ellis et al. 2014; Yanagisawa et al. 2014). Currently, RNA-Seq has been widely employed as a powerful approach to study the transcriptional levels of genes in plants (Pradhan et al. 2014), bacteria (Liu et al. 2014; Mazin et al. 2014), and mammalian cells (Li et al. 2015) due to its higher sensitivity and ability to identify novel genes, transcripts, and single-nucleotide polymorphisms (SNPs).

The primary objectives of this study were to investigate the molecular mechanisms underlying MO biodegradation by strain MR-1 under microaerophilic conditions and to explore the genetic mechanisms involved in azoreduction inhibition caused by DO under aerobic conditions. ^{1}H NMR metabolome and RNA-Seq analyses were performed to reveal bacterial metabolic profiles and gene transcription levels, respectively. The results of this study allow us to gain a systematic understanding of the mechanism underlying azo dye biodegradation by bacteria under different conditions.

Materials and methods

Strain and culture conditions

The MO-degrading strain *S. oneidensis* MR-1 (ATCC® 700550™) was granted by Prof. Haichun Gao of Zhejiang University. Strain MR-1 was inoculated into 30 mL of liquid discoloration medium, containing 1.0 g L^{-1} lactose, 2.0 g L^{-1} sodium lactate, 1.5 g L^{-1} KH_2PO_4, 0.5 g L^{-1} NaCl, and 0.1 g L^{-1} NH_4Cl, and was cultured in an shake incubator maintained at 30 °C. To unravel the mechanisms involved in metabolic and transcriptional changes caused by MO and DO, strain MR-1 was incubated in 30 mL of liquid discoloration medium under three different conditions: microaerophilic conditions with MO (MAMO), microaerophilic conditions without MO (MA), or aerobic conditions with MO (AMO). Microaerophilic conditions were implemented by maintaining the incubator under static conditions, during which the concentration of DO in the flasks varied between 0.9 and 1.6 mg L^{-1} (Işik and Sponza 2003). Aerobic conditions were implemented by holding the incubator at a rotation rate of 180 rpm, during which the concentration of DO in the flasks varied between 4.8 and 7.2 mg L^{-1} (Işik and Sponza 2003). DO concentration was determined as previously reported (Carbo et al. 2015). One 150-mL Erlenmeyer flask with a plastic sealing membrane was used for each sample in the MA and MAMO groups and flasks with gauze were used for the AMO group. Eight replicates under each culture condition were prepared for metabolome analysis, and two replicates under each culture condition were used for transcriptome analysis.

Sample preparation for ^{1}H NMR

Based on our experimental results, strain MR-1 entered exponential phase within 3 h in all three treatment groups (Fig. S1 in the Supplementary Material), and the degradation ratio of MO under MAMO conditions was approximately 80% (Fig. S2 in the Supplementary Material). Therefore, bacterial samples were collected after 3 h of cultivation. The flasks were first chilled on ice to quench metabolism, and then, bacterial cells were harvested. Metabolite extraction was performed as previously described (He et al. 2014). After methanol removal in vacuo, all extracts were lyophilized overnight. Solid extracts were reconstituted in 600 μL of a Na^+/K^+ phosphate buffer containing 80% D_2O, 0.001% sodium 3-trimethylsilyl [2,2,3,3-d_4] propionate (TSP), and 0.01% NaN_3. After centrifugation at 4 °C for 20 min, the supernatants were transferred into 5-mm NMR tubes for NMR analysis.

^{1}H NMR spectra acquisition

The NMR spectra of 24 samples were recorded at 600.13 MHz on a Bruker Avance III 600-MHz spectrometer with a cryogenic probe (Bruker BioSpin, Karlsruhe, Germany). A standard ^{1}H NMR spectrum was obtained at 298 K by employing the first increment of the NOESY pulse sequence (RD-90°-t_1-90°-t_m-90°-acquisition; RD = 2 s, t_1 = 4 μs, t_m = 200 ms). The 90° pulse length was set to 11.5 μs. Water suppression was achieved through presaturation at the water resonance frequency. For each

spectrum, 128 transients were collected into 32 K data points with a spectral width of 20 ppm. For further resonance assignments, a series of 2D NMR spectra including ^{1}H-^{1}H correlation spectroscopy (COSY), ^{1}H-^{1}H total correlation spectroscopy (TOCSY), ^{1}H-^{13}C heteronuclear multiple bond correlation (HMBC), and ^{1}H-^{13}C heteronuclear single-quantum correlation (HSQC) was acquired (Ye et al. 2012).

NMR data processing and multivariate data analysis

An exponential window function with a 1-Hz line broadening factor was added to the free induction decays (FIDs) prior to Fourier transformation. All ^{1}H NMR spectra were manually phased, baseline-corrected, and calibrated to TSP (δ 0.00) using Topspin (V3.0, Bruker BioSpin, Karlsruhe, Germany). Data integration was carried out by dividing the spectrum from 9.7 to 0.5 ppm into discrete regions with a wide bucket of 0.004 ppm (2.4 Hz) using the AMIX package (V3.9.2, Bruker BioSpin, Karlsruhe, Germany). The region from 4.7 to 4.9 ppm was abandoned to eliminate the effects of the residual water signal. Data normalization was performed based on the volumes and optical density (OD) values of the bacteria cultures. Following normalization, multivariate data analysis was conducted using the SIMCA-P^{+} package (v11.0 and v12.0, Umetrics AB, Umea, Sweden). Principal component analysis (PCA) was performed to identify outliers within the mean-centered NMR data. Orthogonal projection to latent structure discriminant analysis (OPLS-DA) models were subsequently constructed with the normalized ^{1}H NMR spectra data. Models were validated through a sevenfold cross-validation method (Bylesjo et al. 2006) and were further validated by cross-validation (CV)-ANOVA (Eriksson et al. 2008). The quality and reasonability of the model were monitored by parameters Q^2 (predicted ability) and R^2 (interpret ability). For statistical analysis, the cutoff value used in this study was 0.707. A Q^2 value greater than 0.707 and a p value smaller than 0.05 (obtained from CV-ANOVA) indicated that the OPLS-DA model was valid. Loadings indicating the metabolites responsible for differentiation were calculated via back-transformation (Cloarec et al. 2005) and were plotted with a color-coded correlation coefficient (r) using Matlab Scripts (the MathWorks, Natick, USA). The absolute value of the correlation coefficient ($|r|$) is represented by different colors in the coefficient plot. Warm colors (e.g., red) indicate greater significance of the differentiation contributed by variations between groups than cold colors (e.g., blue).

Sample preparation for RNA-Seq analysis

Individual cultures of strain MR-1 were rapidly transferred into 50-mL centrifuge tubes after 3 h of cultivation, followed by centrifugation at 8000 rpm (4 °C) for 10 min; supernatants were subsequently discarded. Total RNA extraction was carried out using an RNAiso Plus Kit (Takara, Dalian, China). RNA concentrations were determined using Nanodrop (Thermo Fisher Scientific, Waltham, USA), and RNA quality was checked by non-denaturing agarose gel electrophoresis. To obtain qualified complementary DNA (cDNA), the concentrations of RNA are at least 300 ng μL^{-1} and the lanes of 16S and 23S on the gel must be clear and intact. Following DNase I treatment, the GeneRead ribosomal RNA (rRNA) Depletion Kit (QIAGEN, Frankfurt, Germany) was used to remove rRNAs. mRNA was fragmented into short fragments in fragmentation buffer (Thermo Fisher Scientific, Waltham, USA). The cleaved RNA fragments were used as templates to amplify the first-strand cDNA (First-Strand cDNA Synthesis Mix Kit, TransGen, Beijing, China). The second strand synthesis was conducted using DNA Polymerase I and RNase H. The resulting fragments were resolved in elution buffer for end reparation, single-nucleotide adenine addition, and ligation of adapters. Following quantification and qualification of the cDNA library by using Agilent 2100 Bioanalyzer (Agilent, Santa Clara, USA) and ABI StepOnePlus Real-Time PCR System (Thermo Fisher Scientific, Waltham, USA), the library was sequenced using Illumina HiSeq™ 2000 (Illumina, San Diego, USA).

Transcriptome data processing and analysis

Raw reads produced by Illumina HiSeq™ 2000 underwent quality control (see detailed information in the Supplementary Material) and were then filtered into clean reads, which were aligned to the reference genome of *S. oneidensis* MR-1 (GenBank accession: NC_004347). The alignment data were utilized to calculate the distribution of reads on reference genes and the mapping ratio. To screen differentially expressed genes (DEGs), PCA and correlation analysis were performed to achieve deep data processing. The Noiseq software package, which can identify positive changes and false-positive changes, was applied to reveal the DEGs between AMO and MAMO and between MAMO and MA as previously described (Tarazona et al. 2011). DEGs were defined based on the criteria of $M \geq 2$ (or $\log_2$ ratio ≥1) and $p \geq 0.8$, of which M indicates the fold change and p indicates the probability. Clean data obtained from RNA-Seq have been deposited in the NCBI Sequence Read Archive database (accession: SRA486119).

RT-qPCR verification of transcriptome data

To verify the validity of the transcriptome data, the expression levels of 20 genes under both MAMO and AMO conditions were verified by RT-qPCR. The reaction system was 20 μL, containing 10 μL of SYBR Premix Ex Taq (Takara, Dalian, China) 1 μL of primers, 1 μL of cDNA, and 8 μL of ddH_2O.

Specific primers (Table S1 in the Supplementary Material) were designed using the NCBI-Primer BLAST tool (see detailed information in the Supplementary Material). The 16S rRNA gene was employed as the internal standard and was amplified using the primers F1369 (CGGTGAATACGTTC YCGG) and R1492 (GGWTACCTTGTTACGACTT). The $\log_2^{2-\Delta\Delta CT}$ method was applied to calculate gene expression levels. Correlation analysis of data obtained from RNA-Seq and RT-qPCR is displayed in the Supplementary Material (Fig. S3).

Results

^{1}H NMR spectra of intracellular extracts from strain MR-1

Typical ^{1}H NMR spectra for the intracellular extracts obtained from the three treatment groups are shown in Fig. 1. Metabolite resonances were assigned based on 2D NMR incorporating both ^{1}H and ^{13}C data (Table S2 in the Supplementary Material) and were further verified according to the literature (Fan 1996; Fan and Lane 2008). A total of 25 metabolites were identified, including mannose, lipoprotein lipids, aliphatic organic acids (lactate, acetate, succinate and formate), amino acids (alanine, glutamate, and allothreonine), nucleosides and nucleotide metabolites (uracil, uridine, cytidine, adenosine, guanosine, adenosine 2′,3′-cyclic phosphate, and NAD^+), amines (putrescine, acetamide, ethanolamine, *O*-phosphoethanolamine, and propan-2-amine), alcohols (methanol and isopropanol), acetoin, and isoamyl acetate .

Metabolite changes caused by MO and DO

To gain further insight into differential metabolites by strain MR-1 under different culture conditions, a multivariate data analysis was performed. OPLS-DA comparisons between AMO and MAMO as well as MAMO and MA were carried out. The scores and corresponding coefficient plots for dominant metabolites are shown in Fig. 2. In total, the concentrations of nine metabolites significantly increased ($p < 0.05$) under AMO conditions compared with those concentrations under MAMO conditions (Table 1). Among these nine metabolites, NAD^+, an important coenzyme, showed the most positive change with a correlation coefficient ($|r|$) of 1.49. The concentrations of putrescine and lipoprotein lipids also significantly increased ($p < 0.05$) under aerobic conditions (with $|r|$ values of 1.32 and 1.26, respectively). However, metabolite concentrations under MAMO conditions exhibited no significant changes ($p > 0.05$) compared with those under MA conditions (data not shown). These changes are most likely

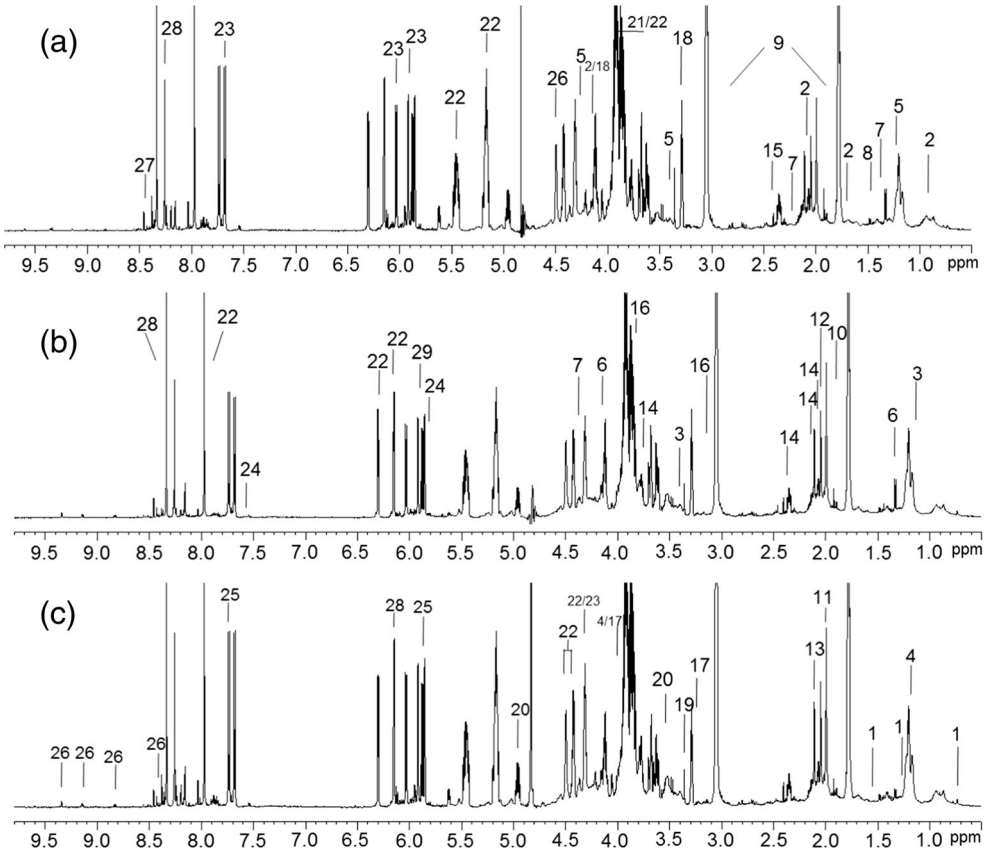

Fig. 1 Typical 600 Hz ^{1}H NMR spectra of extracts from *S. oneidensis* MR-1 grown under MA (**a**), MAMO (**b**), and AMO (**c**) conditions in 30 mL of liquid discoloration medium ($n = 8$). Resonance assignments are listed in Table S1 in the Supplementary Material

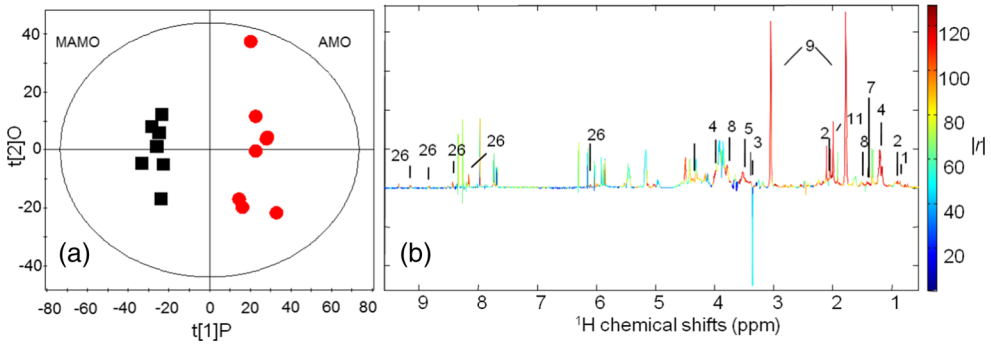

Fig. 2 OPLS-DA score (**a**) and coefficient-coded loading plot (**b**) obtained from ^{1}H NMR data for *S. oneidensis* MR-1 aqueous extracts under AMO (*black squares*) and MAMO (*red dots*) conditions. *t[2]O* cross-validated score value, *t[1]P* model score value. In the loading plot, *red* indicates significantly increased ($p < 0.05$) metabolites and *blue* indicates no significant changes ($p > 0.05$). The metabolite key is displayed in Table 1 (Color figure online)

explained by the recovery of MR-1 under MAMO conditions, accompanied by the biodegradation of MO over time.

DEGs due to MO exposure

Over 4000 genes were detected and analyzed in each sample, within which 145 expressed genes were upregulated and 26 genes were downregulated under MAMO compared to MA conditions (Fig. 3a). DEGs related to certain crucial metabolic processes under MAMO conditions are shown in Fig. 4a. In the presence of MO, the expression levels of gene *azo*R (encoding azoreductase) underwent a significant increase ($\log_2$ ratio (MAMO/MA) = 4.26, $p > 0.8$). Gene *SO1755* (encoding phosphoglucomutase) and *yqh*D (encoding alcohol dehydrogenase) were upregulated, indicating improved glucose metabolism. Transcriptional levels of gene *acn*D (encoding aconitase), which is associated with the tricarboxylic acid (TCA) cycle, also increased. In terms of amino acid metabolism, genes involved in the biodegradation of lysine (*liu*E), leucine (*liu*B/D), phenylalanine (*hpp*D, *phh*A, *hmg*A), isoleucine (*ivd*A/C/E), valine (*ivd*B/F), and histidine (*hut*U) were upregulated. However, the expression of *arg*A and *arg*B, which are responsible for arginine biosynthesis, declined. The expression levels of *arg*F (encoding ornithine carbamoyltransferase), which is involved in the urea cycle, were also reduced. Notably, the expression levels of *yce*J, encoding cytochrome (Cyt) b_{561}, and *bfd*, which encodes (2Fe-2S)-binding protein, were enhanced, implying an incremental requirement for the redox process of in strain MR-1 under MAMO conditions.

Table 1 Significantly changed metabolites in *S. oneidensis* MR-1 growing under AMO conditions compared to MAMO conditions

Metabolites	*r* (AMO vs MAMO)[a]
Lipoprotein lipids	1.26
Isoamyl acetate	1.19
Isopropanol	1.24
Allothreonine	1.24
Acetoin	1.29
Alanine	1.27
Putrescine	1.32
NAD^+	1.49

[a] The positive values of the correlation coefficients indicate increase in the concentration of metabolites. *p* was equal to 0.05. |*r*| equal to 0.707 was used as the corresponding cutoff value of the correlation coefficient for the statistical significance based on the discrimination significance. For AMO vs MAMO, $R^2X = 0.677$, $Q^2 = 0.779$, and $p = 0.0243$. The value of R^2X depicts the goodness of the model, and Q^2 indicates the predictable ability of the model

DEGs caused by a high concentration of DO

Compared with MAMO conditions, 312 genes were upregulated and 759 genes were downregulated (Fig. 3b) under AMO conditions. The DEGs taking part in certain crucial metabolic processes are shown in Fig. 4b, c. Transcriptional levels of *azo*R significantly declined under AMO conditions ($\log_2$ ratio (AMO/MAMO) = −1.9, $p > 0.8$). The expression levels of glyceraldehyde 3-phosphate dehydrogenase (*gap*A) were downregulated (Fig. 4b), whereas gene *gap*B, which encodes the same product as *gap*A, was upregulated (Fig. 4b), suggesting balanced glycolysis. Downregulation of genes *acn*D and *suc*D (encoding succinyl-CoA synthase) resulted in a weakened TCA cycling rate. However, upregulation of genes encoding argininosuccinate synthase (*arg*G) and encoding argininosuccinate lyase (*arg*H) indicated elevated activity of the urea cycle. Genes *fad*E2 and *fad*A/I, related to fatty acid oxidation, were notably upregulated. Amino acid biodegradation rate may be greatly reduced under AMO conditions, which is reflected in the downregulation of *ivd*A/B/C and *liu*A/B/D/E. In addition, amino acid biosynthesis may be improved under AMO conditions, suggested by upregulation of *glt*B/D, *asn*B, *arg*A/B, *thr*A/B/C, *leu*A/B/C/D, *trp*D/E/G, *his*B/C/G, and *ilv*D/G/M, which are responsible for the

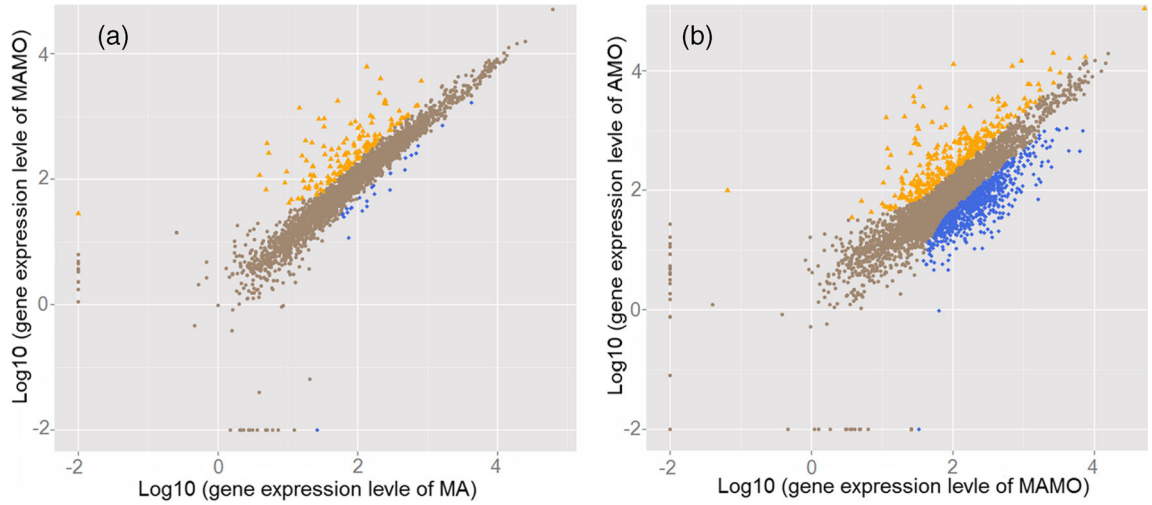

Fig. 3 Scatter plot of all expressed genes under MAMO compared to MA (**a**) and AMO (**b**) compared to MAMO conditions ($n = 2$). *Orange triangles* indicate significantly upregulated genes, and *blue squares* indicate significantly downregulated genes ($M \geq 2$, $p \geq 0.8$). *Gray dots* indicate no significant changes ($M < 2$) (Color figure online)

biosynthesis of glutamate, asparagine, arginine, threonine, leucine, tryptophan, histidine, and isoleucine, respectively. Expression of the genes encoding DNA primase (*dna*G), DNA replication protein (*rep*A), and DNA mismatch repair protein (*mut*L) greatly increased, which signified improved DNA replication processes. Significant reductions ($M \geq 2$, $p \geq 0.8$) in the genes responsible for electron transfer were observed as well, including *yce*J, *frd*B (fumarate reductase), *nuo* (NADH dehydrogenase), *omc*A (Cyt c), *fdx* (2Fe-2S ferredoxin), and *fdh*T (Cyt c oxidase).

Discussion

Effects of MO exposure on bacterial metabolism

Changes in glycolysis in various bacteria have been reported in response to diverse environmental stresses. For example, alterations have been shown in *Escherichia coli* (Payen et al. 2016; Rui et al. 2010) and *Staphylococcus aureus* (Lechnera et al. 2014). In this study, increased expression of phosphoglucomutase (*SO1755*), which is responsible for converting glucose-1-phosphate (G1P) into glucose-6-phosphate (G6P), was clear evidence of improved glycolysis activity. Moreover, the increased levels of aldehyde dehydrogenase (*exa*C, Fig. 4a) and alcohol dehydrogenase (*yqh*D, Fig. 4a) reflected accelerated glycolysis as well (Fig. 5). Based on these observations, we deduced that MO (even at 0.1 g L^{-1}) stress induces MR-1 to consume greater amount of glucose to supply energy.

Bacteria generally regulate amino acid metabolism under adverse conditions (Seo et al. 2013). In this study, increased amino acid biodegradation was observed at the transcriptional level. However, a slight but not significant decrease ($p > 0.05$) in the concentration of amino acids produced by MR-1 occurred in response to MO exposure (Table S3 in the Supplementary Material). This may occur because biodegradation in response to MO over time allows MR-1 to gradually return to a normal growth state (Figs. S1 and S2 in the Supplementary Material). Rapid amino acid biodegradation inevitably produces sufficient acetyl-CoA (lysine, phenylalanine and leucine) and succinyl-CoA (methionine, isoleucine and valine), which are shunted into the TCA cycle (Fig. 5) and improve this process.

The urea cycle and the TCA cycle play important roles in nitrogen metabolism and carbon metabolism, respectively, and these cycles are frequently coupled via a shared source of fumarate (Allen et al. 2011). In this study, acceleration of the TCA cycle (*acn*D) and deceleration of the urea cycle (*arg*F) were noted. The TCA cycle is commonly accelerated during the degradation of hazardous organic pollutants (Seo et al. 2013). Obvious changes of TCA cycle in the present study were in accordance with observations obtained in *Rhodococcus* sp. strain YYL during tetrahydrofuran degradation (He et al. 2014). Alterations in the TCA cycle may directly or indirectly result in the upregulation of aldehyde dehydrogenase and acetyl-CoA synthetase (*acs*, which converts acetate into acetyl-CoA, Figs. 4a and 5). Deceleration of the urea cycle slows down fumarate utilization. This reduction may also be responsible for decreased arginine biosynthesis (*arg*A and *arg*B).

In addition to increased azoreductase (*azo*R) levels, the presence of MO also induced an elevation in cytochrome b_{561} (*yce*J)- and (2Fe-2S)-binding protein (*bfd*) levels, which are primarily associated with complexes of the respiratory electron transfer chain. Azo dye degradation was previously assumed to an extracellular electron transfer process involving

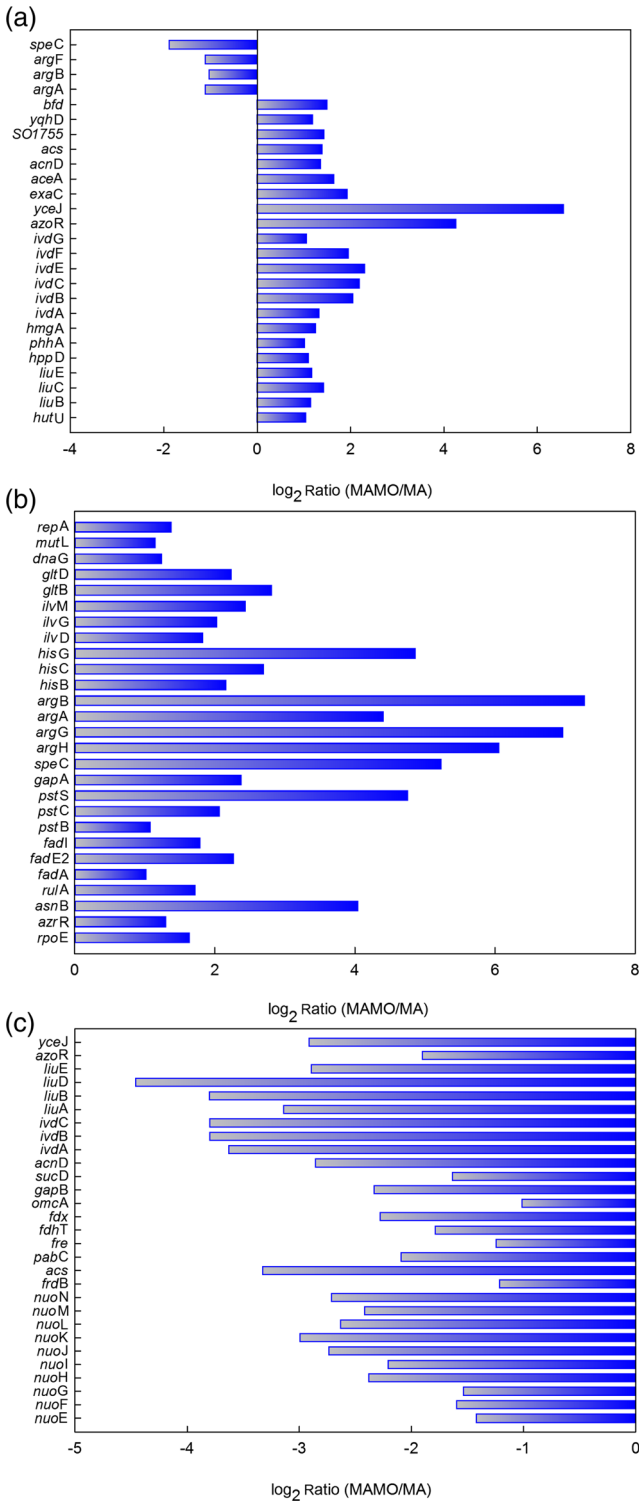

Fig. 4 Partial DEGs under MAMO (**a**) and AMO (**b**, **c**) conditions. Log_2 ratio values are greater than 1, indicating $M \geq 2$. Positive values indicate upregulation, and negative values indicate downregulation. The probability (p) is greater than 0.8

multicomponents located on membrane (Brige et al. 2008; Hong et al. 2007). Thus, azoreduction may be closely related to the respiratory chain.

Effects of a high concentration of DO on bacterial metabolism

A prominent finding in this study was the acceleration of fatty acid oxidation caused by a high concentration of DO. Long-chain fatty acid oxidation is the primary pathway that supplies energy for bacteria and certain protists (Kim et al. 1989). Therefore, the notable enhancement of acyl-CoA dehydrogenase (*fad*E2) and β-ketoacyl-CoA thiolase (*fad*I/A) was potentially triggered by high energy demands for MR-1 to maintain normal growth. Additionally, the obvious accumulation of lipoprotein lipids, alanines, NAD^+, and putrescine was observed under AMO conditions. Lipoprotein lipids are important components of the cell membrane. In bacteria, under certain circumstances, alanine serves as a growth factor to improve growth levels (Snell and Guirard 1943). NAD^+ may be involved not only in glycolysis and the TCA cycle to produce NADH, but also in DNA replication and DNA mismatch repair processes (Fouquerel and Sobol 2014). Putrescine, whose increase may be attributable to the upregulation of ornithine decarboxylase (*spe*C, Fig. 4b), plays an essential role in bacterial DNA, RNA, and protein biosynthesis as well as cell division (Ando et al. 1994). Since biomass of facultative anaerobe is usually greater when they are incubated under aerobic conditions than under microaerophilic conditions (Romano et al. 2015), increases in these metabolites may be primarily related to bacterial growth because more biomass was produced under AMO conditions (Fig. S1 in the Supplementary Material). Moreover, the increased demand for putrescine accompanying bacterial growth may enhance the urea cycle under AMO conditions (Fig. 5).

According to a previous study, increased allothreonine reflects drastic amino acid synthesis and cell growth (Jhee et al. 2002). Thus, the accumulation of allothreonine (Table 1) and the upregulation of genes responsible for amino acid biosynthesis suggest that strain MR-1 under AMO conditions was starved for amino acids. Moreover, improved amino acid biosynthesis may be responsible for reductions in the TCA cycle (*acn*D and *suc*D) due to the consumption of 2-ketoglutarate, oxaloacetate, and pyruvate (Fig. 5). For instance, the accumulation of acetoin (Table 1) under AMO conditions was accompanied by the mass depletion of pyruvate (Xiao and Lu 2014); accelerated arginine biosynthesis (*arg*A and *arg*B) may also result in enhancement of the urea cycle. Amino acid metabolism, the TCA cycle, and the urea cycle generally interact with each other in bacteria during cell growth (Tremaroli et al. 2009).

In addition to the drop in azoreductase, another prominent finding was the decreased expression levels of Cyt b_{561} (*yce*J), NADH dehydrogenase (*nuo*), 2Fe-2S ferredoxin (*fdx*), Cyt c (*omc*A), and Cyt c oxidase (*fdh*) under AMO conditions. All of these proteins are involved in the respiratory electron transfer chain. Thus, higher DO appears to heavily impact the

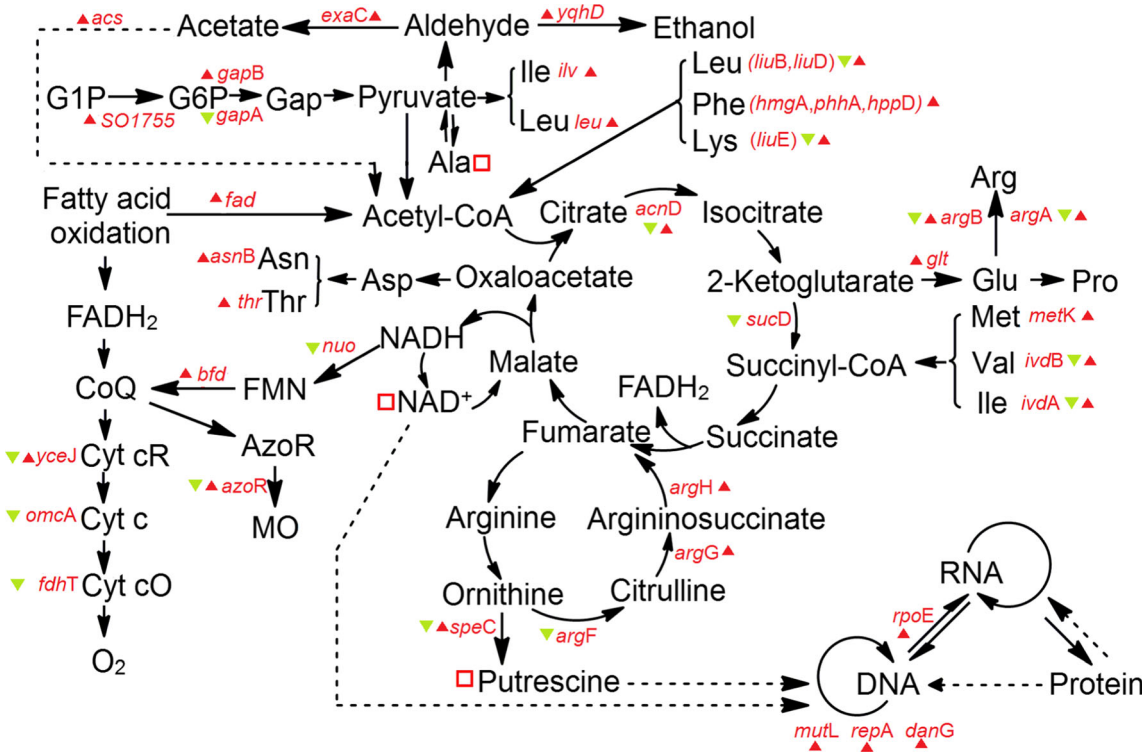

Fig. 5 Alterations in metabolic pathways of *S. oneidensis* MR-1 under AMO and MAMO conditions. Genes, abbreviations, and symbols: *fad* includes *fad*A, *fad*I, and *fad*E2. *thr* includes *thr*B and *thr*C. *ilv* includes *ilv*G, *ilv*M, and *ilv*D. *leu* includes *leu*A, *leu*B, *leu*C, and *leu*D. *glt* includes *glt*D and *glt*B. *G1P* glucose-1-phosphate, *G6P* glucose-6-phosphate, *AzoR* azoreductase, *CoA* ubiquinone, *Cyt* cytochrome, *Cyt cR* cytochrome c reductase, *Cyt cO* cytochrome c oxidase; *red triangles*, significant upregulation ($M \geq 2$, $p \geq 0.8$); *green inverse triangles*, significant downregulation; *red squares*, significantly increased metabolites ($p > 0.05$) (Color figure online)

respiratory electron transfer chain in strain MR-1, which may be responsible for the inhibition of MO reduction.

Proposed mechanism underlying MO biodegradation and inhibition by DO

Azoreductase in *S. oneidensis* MR-1 is FMN-dependent and preferred by NADH as an electron donor (Yang et al. 2013). Therefore, based on our observations in this study, we made the following assumptions: (1) azoreductase anchored on the plasma membrane is likely combined with complex I, and (2) azoreduction is a short electron process that overlaps with the initial section of the respiratory electron transfer chain (Fig. 6). During MO biodegradation, dioxygen may compete with MO as an electron acceptor. Under MAMO conditions, the enhancement of the TCA cycle provides more NADH to the electron transfer chain (Fig. 5), which, together with the increase in Cyt b_{561}, enhances the overall electron transfer from NADH to both MO and dioxygen. Meanwhile, the concentration of DO under MAMO conditions was low enough and did not compete with MO as a final electron acceptor. However, under AMO conditions, the decreases in NADH dehydrogenase and the TCA cycle inevitably diminished overall electron transfer from NADH to MO and higher concentration of DO

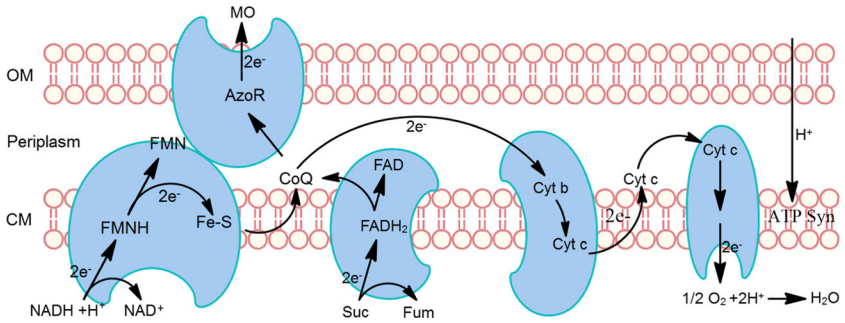

Fig. 6 A hypothetical pathway for azoreduction coupled with complex I (NADH-Q) of the respiratory chain in *S. oneidensis* MR-1. *CoQ* coenzyme Q or ubiquinone, *AzoR* azoreductase, *MO* methyl orange, *Suc* succinate, *Fum* fumarate, *Cyt* cytochrome, *ATP Syn* ATP synthase complex, *OM* outer membrane, *CM* cytoplasmic membrane

under AMO conditions may lead to greater electron flux to dioxygen rather than to MO. Furthermore, the large amounts of $FADH_2$ produced by fatty acid oxidation under AMO conditions directly participate in electron transfer to generate adenosine triphosphate (ATP), potentially accelerating the flux of electrons from coenzyme Q (CoQ) to dioxygen as well (Figs. 5 and 6). The decrease in FMN reductase (*fre*, converting $FMNH_2$ to FMN, Fig. 4c) under AMO conditions may also result in reduced azoreduction.

In summary, the findings in this study revealed the following: (1) an integrated relationship between crucial metabolic processes and MO biodegradation, and (2) in terms of MO degradation, strain MR-1 showed a tendency to maintain growth in the presence of high concentrations of DO.

Acknowledgements This work was supported in part by the National Natural Science Foundation of China (NO. 31400113), Funding Project of Sino-Africa Joint Research Center, Chinese Academy of Sciences (Y623321K01), and the Hundred Talents Program of the Chinese Academy of Science (Y329671K01).

Compliance with ethical standards

Conflict of interest The authors declare that they have no conflict of interest.

Ethical approval This article does not contain studies with human participants or animals by any of the authors.

References

Allen AE, Dupont CL, Obornik M, Horak A, Nunes-Nesi A, McCrow JP, Zheng H, Johnson DA, Hu HH, Fernie AR, Bowler C (2011) Evolution and metabolic significance of the urea cycle in photosynthetic diatoms. Nature 473(7346):203–207

Ando T, Endo Y, Abe M, Kumagai K (1994) Stimulation of the synthesis of histamine and putrescine in mice by a peptidoglycan of gram-positive bacteria. Microbiol Immunol 38(3):209–215

Brige A, Motte B, Borloo J, Buysschaert G, Devreese B, Van Beeumen JJ (2008) Bacterial decolorization of textile dyes is an extracellular process requiring a multicomponent electron transfer pathway. Microb Biotechnol 1(1):40–52

Bylesjo M, Rantalainen M, Cloarec O, Nicholson JK, Holmes E, Trygg J (2006) OPLS discriminant analysis: combining the strengths of PLS-DA and SIMCA classification. J Chemom 20(8–10):341–351

Cao DM, Xiao X, Wu YM, Ma XB, Wang MN, Wu YY, Du DL (2013) Role of electricity production in the anaerobic decolorization of dye mixture by exoelectrogenic bacterium *Shewanella oneidensis* MR-1. Bioresour Technol 136:176–181

Carbo R, Ginovart M, Carta A, Portell X, del Valle LJ (2015) Effect of aerobic and microaerophilic culture in the growth dynamics of *Saccharomyces cerevisiae* and in training of quiescent and non-quiescent subpopulations. Arch Microbiol 197(8):991–999

Cloarec O, Dumas ME, Trygg J, Craig A, Barton RH, Lindon JC, Nicholson JK, Holmes E (2005) Evaluation of the orthogonal projection on latent structure model limitations caused by chemical shift variability and improved visualization of biomarker changes in H-1 NMR spectroscopic metabonomic studies. Anal Chem 77(2):517–526

Ellis RP, Spicer JI, Byrne JJ, Sommer U, Vian MR, White DA, Widdicombe S (2014) H-1 NMR metabolomics reveals contrasting response by male and female mussels exposed to reduced seawater pH, increased temperature, and a pathogen. Environ Sci Technol 48(12):7044–7052

Eriksson L, Trygg J, Wold S (2008) CV-ANOVA for significance testing of PLS and OPLS (R) models. J Chemom 22(11–12):594–600

Fan WMT (1996) Metabolite profiling by one- and two-dimensional NMR analysis of complex mixtures. Prog Nucl Mag Res Sp 28: 161–219

Fan WMT, Lane AN (2008) Structure-based profiling of metabolites and isotopomers by NMR. Prog Nucl Mag Res Sp 52(2–3):69–117

Forgacs E, Cserhati T, Oros G (2004) Removal of synthetic dyes from wastewaters: a review. Environ Int 30(7):953–971

Fouquerel E, Sobol RW (2014) ARTD1 (PARP1) activation and NAD(+) in DNA repair and cell death. DNA Repair 23:27–32

Hafshejani MK, Ogugbue CJ, Morad N (2014) Application of response surface methodology for optimization of decolorization and mineralization of triazo dye Direct Blue 71 by *Pseudomonas aeruginosa*. 3. Biotech 4(6):605–619

He ZX, Yao YL, Lu ZM, Ye YF (2014) Dynamic metabolic and transcriptional profiling of *Rhodococcus* sp strain YYL during the degradation of tetrahydrofuran. Appl Environ Microbiol 80(9):2656–2664

Hong JH, Lee WC, Hsu YM, Liang HJ, Wan CH, Chien CL, Lin CY (2014) Characterization of the biochemical effects of naphthalene on the mouse respiratory system using NMR-based metabolomics. J Appl Toxicol 34(12):1379–1388

Hong Y, Xu M, Guo J, Xu Z, Chen X, Sun G (2007) Respiration and growth of *Shewanella decolorationis* S12 with an azo compound as the sole electron acceptor. Appl Environ Microbiol 73(1):64–72. doi:10.1128/AEM.01415-06

Hu TL (1994) Decolourization of reactive azo dyes by transformation with *Pseudomonas luteola*. Bioresour Technol 49(1):47–51

Işik M, Sponza DT (2003) Effect of oxygen on decolorization of azo dyes by *Escherichia coli* and *Pseudomonas* sp. and fate of aromatic amines. Process Biochem 38(8):1183–1192

Jhee KH, Niks D, McPhie P, Dunn MF, Miles EW (2002) Yeast cystathionine β-synthase reacts with L-allothreonine, a non-natural substrate, and L-homocysteine to form a new amino acid, 3-methyl-L-cystathionine. Biochemistry 41(6):1828–1835

Jin YJ, Li N, Liu HQ, Hua X, Zhang QY, Chen MD, Teng F (2014) Highly efficient degradation of dye pollutants by Ce-doped MoO3 catalyst at room temperature. Dalton T 43(34):12860–12870

Khan R, Khan Z, Nikhil B, Jyoti D, Datta M (2014a) Azo dye decolorization under microaerophilic conditions by a bacterial mixture isolated from anthropogenic dye-contaminated soil. Bioremediat J 18(2):147–157

Khan Z, Jain K, Soni A, Madamwar D (2014b) Microaerophilic degradation of sulphonated azo dye—Reactive Red 195 by bacterial consortium AR1 through co-metabolism. Int Biodeter Biodegr 94:167–175

Kim KH, Lopezcasillas F, Bai DH, Luo X, Pape ME (1989) Role of reversible phosphorylation of acetyl-CoA carboxylase in long-chain fatty-acid synthesis. FASEB J 3(11):2250–2256

Kudlich M, Keck A, Klein J, Stolz A (1997) Localization of the enzyme system involved in anaerobic reduction of azo dyes by *Sphingomonas* sp. strain BN6 and effect of artificial redox mediators on the rate of azo dye reduction. Appl Environ Microbiol 63(9): 3691–3694

Kumari L, Tiwary D, Mishra PK (2016) Biodegradation of C.I. Acid Red 1 by indigenous bacteria *Stenotrophomonas* sp. BHUSSp X2 isolated from dye contaminated soil. Environ Sci Pollut Res Int 23(5): 4054–4062

Le Laz S, Kpebe A, Lorquin J, Brugna M, Rousset M (2014) H2-dependent azoreduction by *Shewanella oneidensis* MR-1: involvement of secreted flavins and both [Ni-Fe] and [Fe-Fe] hydrogenases. Appl Microbiol Biotechnol 98(6):2699–2707

Lechnera S, Praxa M, Lange B, Huber C, Eisenreich W, Herbig A, Nieselt K, Bertram R (2014) Metabolic and transcriptional activities of *Staphylococcus aureus* challenged with high-doses of daptomycin. Int J Med Microbiol 304(8):931–940

Li H, Zhu W, Zhang L, Lei H, Wu X, Guo L, Chen X, Wang Y, Tang H (2015) The metabolic responses to hepatitis B virus infection shed new light on pathogenesis and targets for treatment. Sci Rep 5:8421

Lindon JC, Holmes E, Nicholson JK (2001) Pattern recognition methods and applications in biomedical magnetic resonance. Prog Nucl Mag Res Sp 39(1):1–40

Liu XD, Luo YT, Mohamed OA, Liu DY, Wei GH (2014) Global transcriptome analysis of *Mesorhizobium alhagi* CCNWXJ12-2 under salt stress. BMC Microbiol 14:319

Mazin PV, Fisunov GY, Gorbachev AY, Kapitskaya KY, Altukhov IA, Semashko TA, Alexeev DG, Govorun VM (2014) Transcriptome analysis reveals novel regulatory mechanisms in a genome-reduced bacterium. Nucleic Acids Res 42(21):13254–13268

Payen VL, Porporato PE, Baselet B, Sonveaux P (2016) Metabolic changes associated with tumor metastasis, part 1: tumor pH, glycolysis and the pentose phosphate pathway. Cell Mol Life Sci 73(7): 1333–1348

Pradhan S, Bandhiwal N, Shah N, Kant C, Gaur R, Bhatia S (2014) Global transcriptome analysis of developing chickpea (*Cicer arietinum* L.) seeds. Front. Plant Sci 5:698

Rochfort S (2005) Metabolomics reviewed: a new "omics" platform technology for systems biology and implications for natural products research. J Nat Prod 68(12):1813–1820

Romano S, Schulz-Vogt HN, Gonzalez JM, Bondarev V (2015) Phosphate limitation induces drastic physiological changes, virulence-related gene expression, and secondary metabolite production in *Pseudovibrio* sp strain FO-BEG1. Appl Environ Microbiol 81(10):3518–3528

Rui B, Shen T, Zhou H, Liu JP, Chen JS, Pan XS, Liu HY, Wu JH, Zheng HR, Shi YY (2010) A systematic investigation of *Escherichia coli* central carbon metabolism in response to superoxide stress. BMC Syst Biol 4:122

Saroj S, Kumar K, Prasad M, Singh RP (2014) Differential expression of peroxidase and ABC transporter as the key regulatory components for degradation of azo dyes by *Penicillium oxalicum* SAR-3. Funct Integr Genomic 14(4):631–642

Seo JS, Keum YS, Li QX (2013) Metabolomic and proteomic insights into carbaryl catabolism by *Burkholderia* sp. C3 and degradation of ten N-methylcarbamates. Biodegradation 24(6):795–811

Silva SQ, Silva DC, Lanna MCS, Baeta BEL, Aquino SF (2014) Microbial dynamics during azo dye degradation in a UASB reactor supplied with yeast extract. Braz J Microbiol 45(4):1153–1160

Singh K, Arora S (2011) Removal of synthetic textile dyes from wastewaters: a critical review on present treatment technologies. Crit Rev Env Sci Tec 41(9):807–878

Snell EE, Guirard BM (1943) Some interrelationships of pyridoxine alanine and glycine in their effect on certain lactic acid bacteria. PNAS 29:66–73

Stolz A (2001) Basic and applied aspects in the microbial degradation of azo dyes. Appl Microbiol Biotechnol 56(1–2):69–80

Tarazona S, Garcia-Alcalde F, Dopazo J, Ferrer A, Conesa A (2011) Differential expression in RNA-seq: a matter of depth. Genome Res 21(12):2213–2223

Tremaroli V, Workentine ML, Weljie AM, Vogel HJ, Ceri H, Viti C, Tatti E, Zhang P, Hynes AP, Turner RJ, Zannoni D (2009) Metabolomic investigation of the bacterial response to a metal challenge. Appl Environ Microbiol 75(3):719–728

Tyagi R, Rana P, Gupta M, Bhatnagar D, Srivastava S, Roy R, Khushu S (2014) H-1 NMR spectroscopic analysis detects metabolic disturbances in rat urine on acute exposure to heavy metal tungsten alloy based metals salt. Chem Biol Interact 211:20–28

Wang X, Jin MJ, Balan V, Jones AD, Li X, Li BZ, Dale BE, Yuan YJ (2014) Comparative metabolic profiling revealed limitations in xylose-fermenting yeast during co-fermentation of glucose and xylose in the presence of inhibitors. Biotechnol Bioeng 111(1):152–164

Willetts JRM, Ashbolt NJ (2000) Understanding anaerobic decolourisation of textile dye wastewater: mechanism and kinetics. Water Sci Technol 42(1–2):409–415

Wishart DS (2005) Metabolomics: the principles and potential applications to transplantation. Am J Transplant 5(12):2814–2820

Xiao Z, Lu JR (2014) Strategies for enhancing fermentative production of acetoin: a review. Biotechnol Adv 32(2):492–503

Yanagisawa Y, Piao R, Iguchi S, Nakagome H, Takao T, Kominato K, Hamada M, Matsumoto S, Suematsu H, Jin X, Takahashi M, Yamazaki T, Maeda H (2014) Operation of a 400 MHz NMR magnet using a (RE:rare earth)Ba2Cu3O7-x high-temperature superconducting coil: towards an ultra-compact super-high field NMR spectrometer operated beyond 1 GHz. J Magn Reson 249: 38–48

Yang YY, Lu LL, Gao F, Zhao Y (2013) Characterization of an efficient catalytic and organic solvent-tolerant azoreductase toward methyl red from *Shewanella oneidensis* MR-1. Environ Sci Pollut R 20(5):3232–3239

Ye YF, Zhang LM, Hao FH, Zhang JT, Wang YL, Tang HR (2012) Global metabolomic responses of *Escherichia coli* to heat stress. J Proteome Res 11(4):2559–2566

Zhang LM, Ye YF, An YP, Tian YA, Wang YL, Tang HR (2011) Systems responses of rats to aflatoxin B1 exposure revealed with metabonomic changes in multiple biological matrices. J Proteome Res 10(2):614–623